10474 J. Phys. Chem. A **2009,** *113,* 10474–10487

Modeling TNT Ignition

Michael L. Hobbs,*,[†] Michael J. Kaneshige,[‡] Don W. Gilbert,[§] Stephen K. Marley,[§] and Steven N. Todd[||]

Engineering Sciences Center, Energetic Components Realization, and Systems Assessment and Research, Sandia National Laboratories, Albuquerque, New Mexico 87105

Received: June 30, 2009

A 2,4,6-trinitrotoluene (TNT) ignition model was developed using data from multiple sources.[1−4] The one-step, first-order, pressure-dependent mechanism was used to predict ignition behavior from small- and large-scale experiments involving significant fluid motion. Bubbles created from decomposition gases were shown to cause vigorous boiling. The forced mixing caused by these bubbles was not modeled adequately using only free liquid convection. Thorough mixing and ample contact of the reactive species indicated that the TNT decomposition products were in equilibrium. The effect of impurities on the reaction rate was the primary uncertainty in the decomposition model.

Introduction

Predicting the response of TNT during an accident, such as a fire, is important for high consequence safety analysis. The response may rely upon many factors such as pressure-dependent kinetics, liquid convection, forced convection induced by decomposition, viscosity, volumetric expansion, thermal conductivity, specific heat, and decomposition product composition at elevated temperature and pressure. Knowledge of both the solid and the liquid state of TNT is necessary to predict and mitigate inadvertent thermal ignition. The present work increases our understanding of complex preignition reactions and thermophysical changes in TNT leading to thermal runaway. An overview of thermal runaway leading to ignition can be found elsewhere.[5−7] Postignition burning and resulting violence is beyond the scope of the current article.

TNT is insensitive to shock and friction, melts near 81 °C, and can be cast into many shapes. TNT does not decompose at the melting point and can be solidified without changing the freezing point. However, at higher temperatures, condensed-phase reactions occur in the liquid forming various aromatic compounds, a reactive coke, and small quantities of gas products. At high temperatures, decomposition gases cause vigorous convective heat transfer. Dacons et al.[8] heated TNT to 150 °C for 70 h and observed minor darkening of the resolidified TNT with a melting-point depression of 1 °C. Upon heating TNT to 200 °C, intense darkening of the TNT indicated onset of rapid reaction possibly catalyzed by a “coke” leading to spontaneous self-ignition.

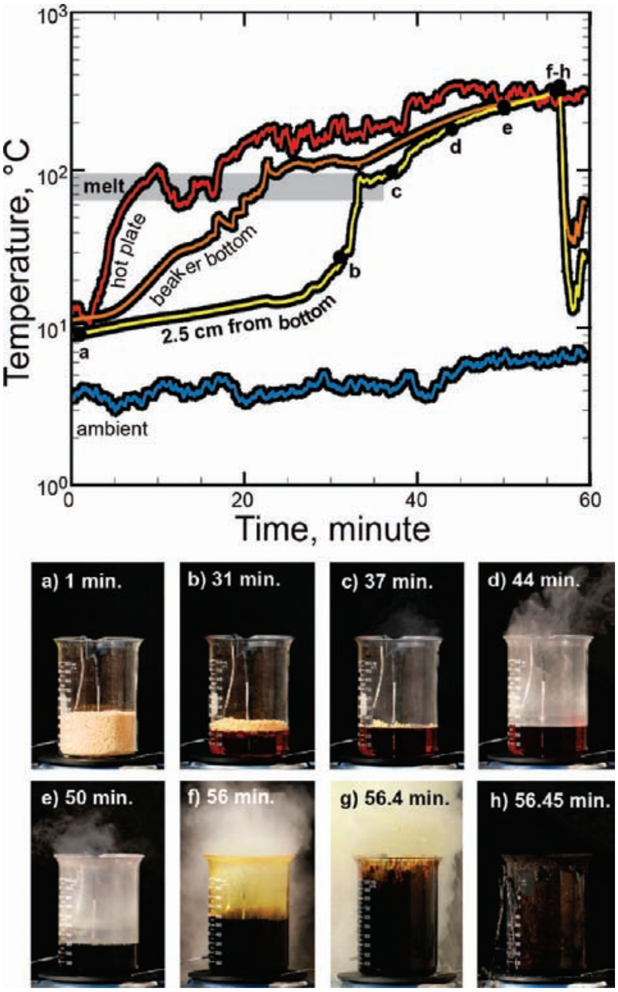

Figure 1. Temperature and images of flaked TNT in a glass flask on a hot plate.

Figure 1 shows the reaction progress of 450 mL of flaked TNT in a glass beaker placed on a hot plate for 1 h. Two thermocouples were placed in the flaked TNT, one at the bottom of the beaker and one 2.5 cm from the beaker bottom. Two additional thermocouples were placed outside the beaker, one on the hot plate and one just outside of the beaker labeled “ambient” in Figure 1. The TNT formed about 300 mL of a red liquid, which began to evolve white smoke as the liquid increased in temperature. At about 200 °C, the liquid turned black, and intense boiling indicated significant reaction.

---

* Corresponding author. E-mail: mlhobbs@sandia.gov.

[†] Engineering Sciences Center, Nanoscale & Reactive Processes Department.

[‡] Energetic Components Realization, Explosive Projects/Diagnostics Department.

[§] Systems Assessment and Research, Energetic Threats & Training Department.

[||] Systems Assessment and Research, Energetic Systems Research.

10.1021/jp906134f CCC: $40.75

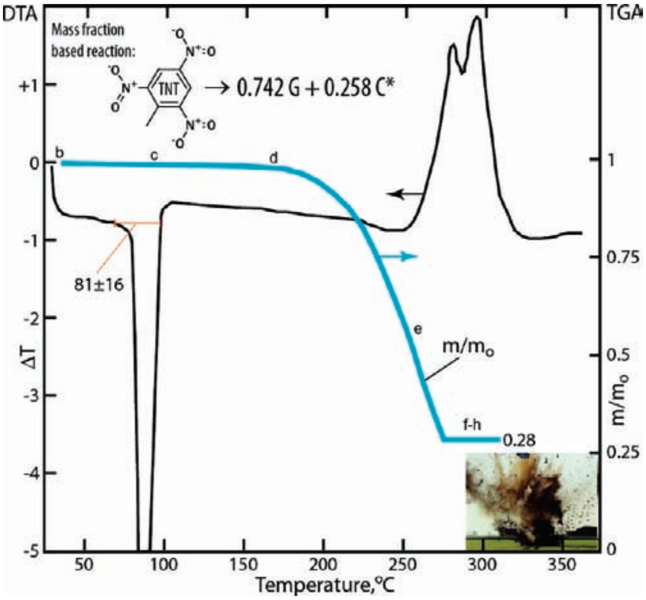

Figure 2. DTA/TGA of TNT.[9] Inset picture of sooty TNT explosion.[11] Mole based reaction scheme is TNT ($C_7H_5N_3O_6$) → 0.18 CH_4 + 2.14 H_2O + 1.93 CO_2 + 1.5 N_2 + 4.89 C. G and C represent gaseous reaction products and carbon, respectively.

Figure 2 shows a differential thermal analysis (DTA) and a thermogravimetric analysis (TGA) for TNT,[9] explaining some of Dacon's observations[8] as well as the reaction sequence shown in Figure 1. TNT melts with a large mush zone, 81 ± 16 °C, there is no endotherm associated with simple TNT boiling (TNT liquid changing to TNT gas), and gas generation does not start until about 175 °C. For a rough comparison, the temperatures located 2.5 cm from the bottom of the glass beaker labeled b−h in Figure 1 are also shown in Figure 2. These temperatures are 28, 98, 181, 254, 317, 325, and 344 °C, respectively, and correspond to pictures b−h at the bottom of Figure 1.

The final residue (28 mass percent) from the TGA experiment is consistent with the decomposition products being in chemical equilibrium with one of the equilibrium products being condensed carbon, as shown in the reaction in the caption of Figure 2. The equilibrium products of TNT at 500 K and 1−50 atm were calculated using the JCZS equation of state.[10] Figure 1 also shows the TNT decomposition reaction based on mass, where the stoichiometric coefficients represent the mass fraction of decomposition gases (0.742) and the mass fraction of condensed carbon (0.258). Also, the inset picture of a black sooty TNT explosion indicates the presence of fuel rich products.

Lee et al.[12] studied fast cookoff of 2.1 mm diameter by 4.7 mm long cylinders of TNT (~0.016 cm^3) at static pressures between 10 and 50 kbar. Lee controlled the TNT sample temperatures to within ±30 °C, observed little dependence on pressure, and concluded that most of the preignition reactions in TNT were liquid-phase reactions. However, the large uncertainty in temperature may have obscured the pressure dependency.

The current work supports a rate-limiting step controlled by catalysis from decomposition products, as discussed further by Brill and James.[13] However, in the current work, a pressure-dependent model fit TNT ignition data better for confined systems with limited free gas volume. Dynamic pressures studied in the current work were much less than those studied by Lee and rarely exceeded 1 to 2 kbar before confinement breach. Boundary temperatures were also controlled to within ±0.1 °C, and some of the experiments included internal temperatures and pressure measurements.

A single acceleratory rate[14] was used to model TNT ignition. A long induction period followed by an accelerating reaction rate was obtained by normally distributing the activation energy with respect to the extent of reaction. Distributed activation energies have been used to describe decomposition of large molecules such as coal,[15] polymers,[16] and more recently, explosives.[17,18] When the extent of reaction is small, the activation energy is high and reaction rates are low. As the extent of reaction increases, the activation energy decreases, leading to acceleratory reaction rates. The remainder of this article describes the model, parameter estimation, various experiments, and model validation.

Model

In typical simulations, thermal ignition of explosives is determined by solving the conductive energy equation using a volumetric source for chemical reactions. This approach is fine for most explosives that do not melt at low temperatures and for small TNT samples. However, for larger TNT samples, liquid convective flow contributes significantly to heat transfer. In the current work, two sets of equations are solved: (1) for small systems where liquid convection is not important and (2) for large systems where liquid convection is important.

For the small quantities of TNT, conductive heat transfer is adequate for the TNT to reach the external boundary temperature rapidly. For larger systems, liquid convection also transports energy from the boundary unto the reactive material. In the current article, only natural fluid motion caused by density and temperature gradients is modeled. Forced fluid motion produced by three-phase (solid, liquid, and gas) reactive flow is beyond the scope of the current article and should be considered for future work.

Tables 1 and 2 present the model without liquid convection and with liquid convection, respectively. The model without liquid convection uses a low Mach flow assumption, where the gas velocity is much less than sound speeds and the pressure within the system is only a function of time, that is, $P(x,y,z,t) = P(t)$. Pressure changes temporally because of increasing temperature and reaction. Condensed and gas-phase temperatures are also assumed to be equal, that is, $T_c = T_g = T(x,y,z,t)$. The model with liquid convection assumes "no slip" between the local condensed and gas phases as well as the container walls and temperature probes. "Slip" is allowed at the interface between the liquid and the air space above the TNT. The inset drawing of the domain in Table 1 shows a more general open system with permeable and impermeable regions. In the current article, only closed, permeable systems are considered. The model equations without and with liquid convection were solved using Calore[19] and Comsol,[20] respectively.

The reaction mechanism and auxiliary equations are the same for both models and are given in Table 3. The TNT material parameters are given in Table 4, and experiment-specific parameters are given in Table 5. Confined decomposition with prolonged contact of reactive species justifies the assumption that decomposing TNT forms equilibrium products. One benefit of the equilibrium assumption is that reaction enthalpy can be specified using Hess's law, and the product gas molecular weight is known.

The form of the effective thermal conductivity in eq 15 of Table 3 has been used by Glicksman[21] for cellular materials. The factor 2/3 describes tortuosity. The absorption coefficients given in Table 4 were chosen on the basis of the absorptivity of polyurethane[22] and air.[23] The solid and liquid thermal conductivity in Table 4 were determined using data from

TABLE 1: TNT Ignition Model without Liquid Convection Showing Domain[a]

Gas continuity (integral)	$\frac{dM_g}{dt} = \int_\Lambda r dm_c^o + \dot{m}_i - \dot{m}_o$	(1)
Gas momentum (low Mach)	$P(x,y,z,t) = P(t) = M_g \Big/ \int_\Lambda \frac{M_{wg}}{RT} d\Lambda$	(2)
Energy (integral: bulk elements)	$\frac{dV_b \rho_g C_g T_b}{dt} = -\int_S h(T_b - T) dS + \dot{m}_i h_i - \dot{m}_o h_o$	(3)
Energy (field: material blocks)	$\rho_b C_b \frac{\partial T}{\partial t} = \nabla \cdot (k \nabla T) + qr$	(4)

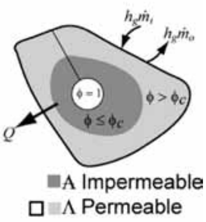

[a] C_b, C_g, h_i, h_o, k, m_c^o, $\dot{m}_i$, $\dot{m}_o$, M_g, M_{wg}, P, q, r, R, S, t, T, T_b, V, x, y, z, ρ_b, ρ_g, ϕ, ϕ_c, and Λ represent bulk specific heat, gas specific heat, influx enthalpy, outflux enthalpy, thermal conductivity, initial condensed mass, influx mass, outflux mass, mass of gas, molecular weight of gas, pressure, reaction enthalpy, reaction rate, gas constant, enclosure surface, time, temperature, bulk element temperature, volume, x coordinate, y coordinate, z coordinate, bulk density, gas density, gas volume fraction, critical gas volume fraction, and permeable region, respectively.

TABLE 2: TNT Ignition Model Including Liquid Convection[a]

TNT continuity (field)	$\frac{d(\varphi_{tnt}\rho_{tnt})}{dt} + \vec{u} \cdot \nabla(\varphi_{tnt}\rho_{tnt}) = -r\rho_b$	(5)
gas continuity (field)	$\frac{d(\varphi_{gas}\rho_{gas})}{dt} + \vec{u} \cdot \nabla(\varphi_{gas}\rho_{gas}) = 0.742 r\rho_b$	(6)
carbon continuity (field)	$\frac{d(\varphi_{carbon}\rho_{carbon})}{dt} + \vec{u} \cdot \nabla(\varphi_{carbon}\rho_{carbon}) = 0.258 r\rho_b$	(7)
energy (field)	$\rho_b C_b \frac{\partial T}{\partial t} + \rho_b C_b \vec{u} \cdot \nabla T = \nabla \cdot (k \nabla T) + qr$	(8)
momentum (field)	$\rho_b \frac{\partial \vec{v}}{\partial t} + \rho_b \vec{u} \cdot \nabla \vec{u} = -\nabla P + \mu \nabla^2 \vec{v} + \rho_b g$	(9)

[a] Nomenclature for this table is the same as that in Table 1, except φ and ρ in eqs 5, 6, and 7 represent the volume fraction and density of TNT, decomposition gases, and carbon, respectively. The density of the carbon products is assumed to be the same as the density of TNT. $\vec{u}$, μ, and g represent the velocity vector, viscosity, and gravitational vector, respectively.

Sandia's instrumented thermal ignition (SITI) experiment.[1] We achieved the transition from solid to liquid thermal conductivity by using a smooth hyperbolic tangent with the same transition width as the phase change width, as shown in footnote "c" of Table 4. The gas thermal conductivity is assumed to be a linear function of temperature using the air thermal conductivity[24] given in Table 4.

The volumetric expansion coefficient[25] (β in Table 4) is for solid TNT. The expansion of liquid TNT is accounted for by the temperature-dependent expression[26] for ρ_l given in Table 4. The change in the density from solid-to-liquid is transitioned using a smooth hyperbolic tangent with the same transition width as the phase change width, as discussed previously. The latent enthalpy is partitioned over this temperature range using an effective capacitance method. The specific heat is assumed to be linearly dependent on temperature using the two bulk specific heats[3] given in Table 4. The specific heat is increased by h_{pc}/w_{pc} in the temperature range, $T_{pc} - (w_{pc}/2) < T < T_{pc} + (w_{pc}/2)$, to account for latent enthalpy.

Figure 3 shows the viscosity of TNT, decomposing TNT, and air. The symbols represent four TNT viscosity data points.[25] The orange line in Figure 3 shows the TNT viscosity volume averaged with the air viscosity near the ignition point. Decomposition gas viscosity is assumed to be the same as the air viscosity. Calculated TNT viscosity decreases as decomposition gases are generated. More data on TNT viscosity are needed.

One-Dimensional Time-to-Explosion (ODTX) Experiments

The Catalano et al.[24,27] ODTX experiment is shown in Figure 4 where preheated aluminum anvils were used to confine 1.27 cm diameter spheres of TNT to 1500 atm. Heaters controlled the temperature of the anvils to ±0.2 K, and the primary measurement was the "time-to-explosion." Figure 4A shows a schematic of the original ODTX apparatus constructed in 1975. Figure 4B shows the newer ODTX apparatus built in 2001.[27] The newer unit has better control of the sample temperature, the copper gasket is closer to the explosive, and the anvil closing speed was faster. In both ODTX experiments, the two anvils are assumed to be in contact with no separation volume. Therefore, the enclosure volume in Table 5 for the ODTX experiments is zero.

TABLE 3: Reaction Mechanism and Auxiliary Equations[a]

mechanism	$\mathrm{TNT(C_7H_5N_3O_6)} \rightarrow 0.18\mathrm{CH_4} + 2.14\mathrm{H_2O} + 1.93\mathrm{CO_2} + 1.5\mathrm{N_2} + 4.89\mathrm{C}$	(10)
reaction rate	$r = \frac{\mathrm{d}}{\mathrm{d}t}(\mathrm{tnt}) = \xi A\left(\frac{P}{P^{\mathrm{o}}}\right)^n \exp[-(E + z\sigma_{\mathrm{E}})/RT]\mathrm{tnt} \quad \text{where} \quad \mathrm{tnt} = \frac{\varphi_{\mathrm{tnt}}\rho_{\mathrm{tnt}}}{(1 - \phi_{\mathrm{o}})\rho_{\mathrm{c,o}}}$	(11)
distribution parameter	$1 - \mathrm{tnt} = \int_{-\infty}^{z} \frac{1}{\sqrt{2\pi}} \exp\left(\frac{-z^2}{2}\right)\mathrm{d}z \quad \text{or} \quad z = \mathbf{norminv}(1 - \mathrm{tnt})$	(12)
gas volume fraction	$\phi = 1 - [S_{\mathrm{f}}(1 - \phi^{\mathrm{o}})\rho_{\mathrm{c}}^{\mathrm{o}}/\rho_{\mathrm{c}}] \quad \text{where} \quad S_{\mathrm{f}} = \mathrm{tnt} + \mathrm{carbon} = \frac{\varphi_{\mathrm{tnt}}\rho_{\mathrm{tnt}} + \varphi_{\mathrm{carbon}}\rho_{\mathrm{carbon}}}{(1 - \phi_{\mathrm{o}})\rho_{\mathrm{c,o}}}$	(13)
bulk density	$\rho_{\mathrm{b}} = \phi\rho_{\mathrm{g}} + (1 - \phi)\rho_{\mathrm{c}} \quad \text{or} \quad \rho_{\mathrm{b}} = \varphi_{\mathrm{TNT}}\rho_{\mathrm{TNT}} + \varphi_{\mathrm{G}}\rho_{\mathrm{G}} + \varphi_{\mathrm{C}}\rho_{\mathrm{C}}$	(14)
thermal conductivity	$k = \phi k_{\mathrm{g}} + \frac{2}{3}(1 - \phi)k_{\mathrm{c}} + \frac{16\sigma T^3}{3[\phi\alpha_{\mathrm{g}} + (1 - \phi)\alpha_{\mathrm{c}}]}$	(15)
bulk viscosity	$\mu = \phi\mu_{\mathrm{g}} + (1 - \phi)\mu_{\mathrm{tnt}}$	(16)

[a] A, carbon, E, k, k_{g}, k_{c}, **norminv**, P, P^{o}, r, R, T, tnt, z, α_{c}, α_{g}, ϕ, ϕ^{o}, π, ρ_{c}, $\rho_{\mathrm{c}}^{\mathrm{o}}$, ρ_{b}, ρ_{g}, σ, σ_{E}, ω_{tnt}, and ξ represent prefactor, carbon mass fraction, activation energy, effective thermal conductivity, gas conductivity, condensed conductivity, inverse of the normal probability distribution function, pressure, initial pressure, reaction rate, gas constant, temperature, TNT mass fraction, cumulative distribution parameter, condensed absorption, gas absorption, gas volume fraction, initial gas volume fraction, pi, condensed density, initial condensed density, bulk density, gas density, Stephan Boltzmann constant, activation energy dispersion, weight fraction of TNT ($\varphi_{\mathrm{tnt}}\rho_{\mathrm{tnt}}/[(1 - \phi_{\mathrm{o}})\rho_{\mathrm{c,o}}]$ for flow equations), and purity rate multiplier, respectively.

ODTX data collected between 1975 and 2002[27] are shown in Figure 5 for different percentages of symmetrical TNT. The smaller symbols in Figure 5 represent data that were considered to be unreliable. The liquid TNT volume is about 14% greater than the solid TNT at room temperature. This large volume change would sometimes result in the leakage of decomposition products, as observed by Tran[27] if the initial TNT densities were greater than the liquid TNT density, which is 1.42 g/cm^3 at 400 K.

Although the recrystallized TNT data in Figure 5 was reported by Tran[27] to be 100 ± 2%, the purity in the current work is taken to be 99 ± 1%. TNT purity has a dramatic affect on the ignition times. For example, for an anvil temperature of 553 K ($1000/T = 1.81$ K^{-1}), the time-to-ignition is 33 and 687 s for 100 and 90% pure TNT, respectively. This 20-fold increase in ignition time has not been observed in other explosives with higher melting points such as RDX with 6% HMX impurities.[17]

Chrisman[29] measured the purity of TNT used for the SITI and midscale experiments to be greater than 99% using gas chromatograph mass spectrometry (GC-MS), which was validated for TNT, 2,4-dinitrotoluene (DNT), and 2,6-DNT. The army handbook[26] lists the maximum impurities formed during the manufacture of TNT at 7.5% and the maximum amounts contained after purification at 3.5%, with actual impurity concentrations being lower. The main contaminants before purification were 2,4,5-TNT (2.5%), 2,3,4-TNT (1.75%), 2,3,6-TNT (0.5%), 2,4-DNT (0.5%), and 2,4,6-trinitrobenzoic acid. Because Chrisman's analysis was validated only for TNT, 2,4-DNT, and 2,6-DNT, the purity of the TNT used in the SITI and midscale tests may be <99% pure, although the ultrapure TNT used in the 4× recrystallized experiments is expected to be near 100% pure because of the white color of the TNT crystals.

Modeling the effect of impurities is not warranted without knowing the identity of the impurities. In the current work, kinetic parameters were obtained using ODTX data for 99% pure TNT. The rate expression was then modified by a multiplier for other impurity levels. Table 4 shows that the rates for 90% pure TNT are 40 times slower than the rates for the 99% pure TNT. Semilog interpolation is used for other purity levels.

Sandia's Instrument Thermal Ignition (SITI) Experiments

The SITI experiment,[1] shown schematically in Figure 6A,B, had type K 76 μm diameter thermocouples located at various radial positions in the center of a 2.54 cm diameter by 2.54 cm tall cylinder of TNT. The outside temperature of the confining aluminum cylinders was maintained at a controlled set point. Typically, the outside temperature of the aluminum confinement was ramped from room temperature until the set point temperature was reached. The ramp rate was controlled so that each experiment reached the set point temperature in 15 min (900 s). The experiment also has a pressure tap to monitor the pressure during the experiment. Figure 6D shows data from run 409. The red line in Figure 6D represents the boundary temperature, which was ramped from room temperature to a given set point temperature in 15 min. The boundary was then held at the set point temperature until thermal runaway.

Figure 7 shows the TNT data collected from the SITI apparatus from March 2006 to January 2009. Three different

TABLE 4: TNT Material Parameters

parameter	description	value
α_c, m^{-1}	condensed absorption coefficient[22]	50 000 ± 10%
α_g, m^{-1}	gas absorption coefficient[23]	100 ± 10%
β	volumetric expansion coefficient[25]	$(5 \times 10^{-5}) + (7.8 \times 10^{-8})(T - 273.15)$
C_{298}, C_{623} J/kg·K	bulk specific heat[3] at 298 and 623 K	1130, 1675[a]
E, J/kg·mol	activation energy[13]	1.42×10^8
h_{pc}, J/kg	phase change (melting) enthalpy[26]	(9.53×10^4) ± 11%
h_r, J/kg	reaction enthalpy[b]	5.4×10^6
k_c, W/mK	condensed thermal conductivity	$k_{fac}[\delta \times k_L + (1 - \delta)k_s]$[c]
k_{fac}	k_c uncertainty multiplier	1 ± 5%
$k_{g,300}$, $k_{g,500}$ W/mK	gas conductivity[24] at 300 and 500 K	0.0263, 0.0407[d]
k_L, W/mK	liquid conductivity to match data	$8 \times k_s$
k_s, W/mK	solid conductivity to match data	0.25
ln A, ln(s^{-1})	natural logarithm of A	26
$\mu_{g,300,800}$, Pa·s	gas (air[24]) viscosity at 300 and 800 K	1.8×10^{-5}, 3.7×10^{-5} [e]
μ_{tnt}, Pa·s	TNT viscosity[25] at 358 and 373 K	0.013, 0.0088[f]
M_{wg}, g/mol	average gas molecular weight	29.3
M_{wgo}, g/mol	initial gas molecular weight (air)	28
n	pressure exponent	0.5
ρ_c, kg/m^3	condensed TNT density	$\delta \times \rho_L + (1 - \delta)\rho_s$[c]
ρ_L, kg/m^3	liquid TNT density[26]	$(1544.6)-(1.016)\ (T - 273.15)$
ρ_{so}, kg/m^3	initial solid TNT density[25]	1654
ρ_s, kg/m^3	solid TNT density	$\rho_{so}/[1 + \beta(T - T_o)]$
σ_E/R, K	normalized act. energy dispersion	1200
T_{pc}, K	melting point[25]	354 ± 1
w_{pc}, K	melting point range (DTA in Figure 1)	10 ± 5
$\xi(\omega_{tnt} = 0.99)$	rate multiplier for 99% pure TNT	1.0[g]
$\xi(\omega_{tnt} = 0.95)$	rate multiplier for 95% pure TNT	0.03[g]
$\xi(\omega_{tnt} = 0.90)$	rate multiplier for 90% pure TNT	0.025[g]

[a] Bulk heat capacity varies linearly between 298 and 623 K with linear extrapolation. [b] Based on equilibrium reaction: TNT → $0.18CH_4 + 2.14H_2O + 1.93CO_2 + 1.5N_2 + 4.89C$ or TNT → 0.742G + 0.258C on a mass basis. [c] $\delta = 0.5 \times \{1 + \tanh[(T - T_{pc})/w_{pc}]\}$ for the transition. [d] Gas thermal conductivity varies linearly between 300 and 500 K with linear extrapolation. [e] Gas viscosity varies linearly between 300 and 800 K with linear extrapolation. [f] TNT viscosity varies linearly between 358 and 373 K with constant extrapolation. [g] Rate multiplier varies logarithmically among purity percentages of 90, 94, and 99%. For example $\xi = 10^{38.05\omega_{tnt}-37.67}$ if $\omega_{tnt} \geq 0.95$, and $\xi = 10^{1.6\omega_{tnt}-3.04}$ if $\omega_{tnt} < 0.95$.

TABLE 5: TNT Experiment Parameters[a]

parameter	description	ODTX	SITI-flaked	SITI-solid	SITI-4X	midscale
h, W/m^{2}K	convection coefficient	0	1	1	1	0
ρ_{bo}, kg/m^3	initial bulk density	1350 ± 12	896 ± 25	1633 ± 1	1557 ± 21	1420[b]
V_{enc}, cm^3	enclosure volume	0	0.605 ± 0.015	1.99 ± 0.02	1.54 ± 0.04	1362[c]
V_{tnt}, cm^3	bulk TNT volume	1.07	12.9	12.9	12.9	1377
V_{tube}, cm^3	pressure tubing volume	0	0.2 ± 10%	0.2 ± 10%	0.2 ± 10%	0
ω_{tnt}	TNT purity[d]	0.90 ± 0.034 0.94 ± 0.02 0.99 ± 0.01	0.994 ± 0.005	0.979 ± 0.005	0.985 ± 0.005	0.98

[a] One-dimensional time-to-explosion (ODTX), Sandia's instrumented thermal ignition (SITI), and "midscale" experiments are described in detail in subsequent sections. [b] Density of liquid TNT at 400 K. [c] Head space above melted TNT at 400 K. [d] SITI purity with uncertainty was estimated. The midscale purity was estimated.

sample types were used in these experiments: (1) pressed solid, (2) four times (4×) recrystallized TNT pressed into a solid, and (3) flaked TNT. Figure 7B shows pictures of each of these sample types. The recrystallized TNT samples were white, and the stock TNT samples were pale yellow.

The legend in Figure 7A indicates that the average densities of the solid, recrystallized solid, and flaked TNT samples were 1633, 1547, and 896 kg/m^3, respectively. Problems due to liquid clogging the tubes and venting were alleviated by increasing the expansion volume for the solid TNT samples. The average gap volumes are listed in the legend of Figure 7A. The gap volume is the volume of one of two gaps in the SITI experiments. There is an expansion gap at the top of the sample, as shown in Figure 6A, and a similar gap at the bottom of the sample. Total gap volume is twice the V_{gap} value listed in Figure 7A.

The start times for each experiment were synchronized, and overall time-to-ignition is plotted in Figure 7A. The abscissa in

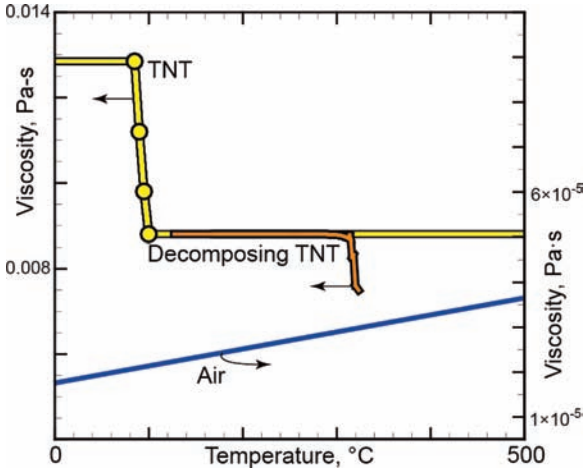

Figure 3. Viscosity of TNT,[25] decomposing TNT, and air.[24]

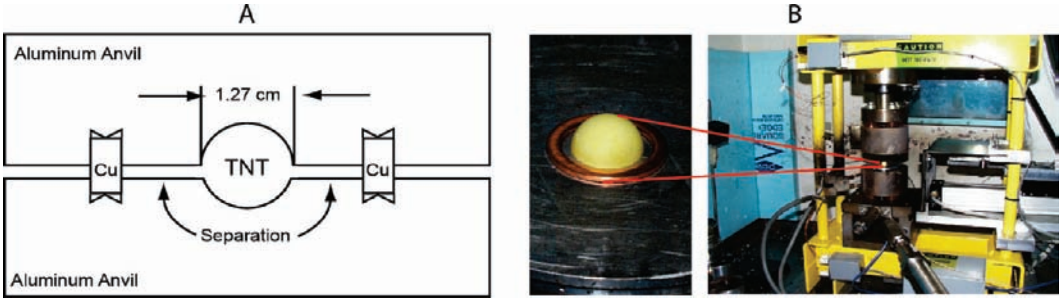

Figure 4. (A) Older ODTX apparatus[2] and (B) explosive in new ODTX apparatus.[27]

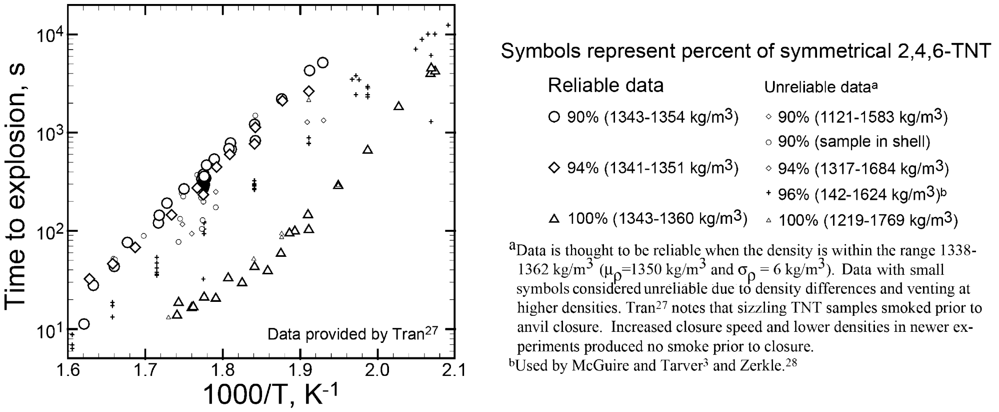

[a] Data is thought to be reliable when the density is within the range 1338-1362 kg/m^3 (μ_ρ=1350 kg/m^3 and σ_ρ = 6 kg/m^3). Data with small symbols considered unreliable due to density differences and venting at higher densities. Tran[27] notes that sizzling TNT samples smoked prior to anvil closure. Increased closure speed and lower densities in newer experiments produced no smoke prior to closure.

[b] Used by McGuire and Tarver[3] and Zerkle.[28]

Figure 5. TNT ODTX data from 1975 to 2002.[27]

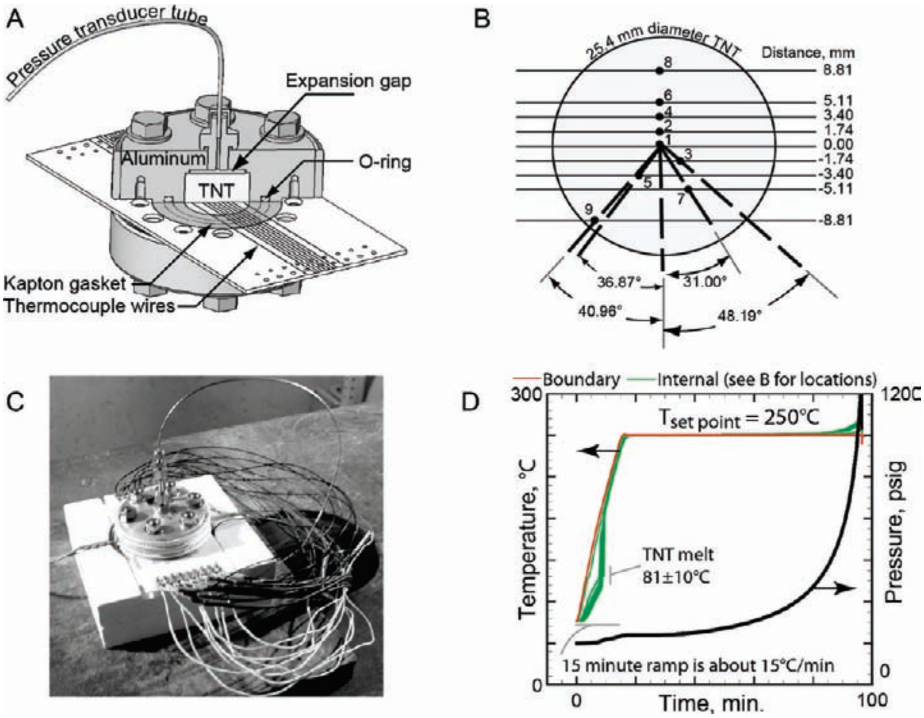

Figure 6. SITI (A) schematic, (B) cross section, (C) picture, and (D) typical boundary temperatures, internal temperatures, and pressure measurement. Example is run 409.

this plot is 1000/T_{setpoint} where T_{setpoint} represents the set point temperature after a 15 min ramp from room temperature. The solid TNT data are represented by solid circles (black for nominally pure TNT and green for 4× recrystallized TNT), and the flaked TNT are represented by open circles. Because of clogging, venting, or other experimental difficulties, 6 of the 18 data points are not considered in the current article. These points are marked with an "×".

Midscale Experiments

Several midscale experiments[30] were used to scale-up and validate the TNT decomposition model. The midscale experiment with 1.95 kg of TNT in a 15 cm diameter by 19 cm tall aluminum cylinder is shown in Figure 8A,B. The picture shows the experiment before being insulated on all outer

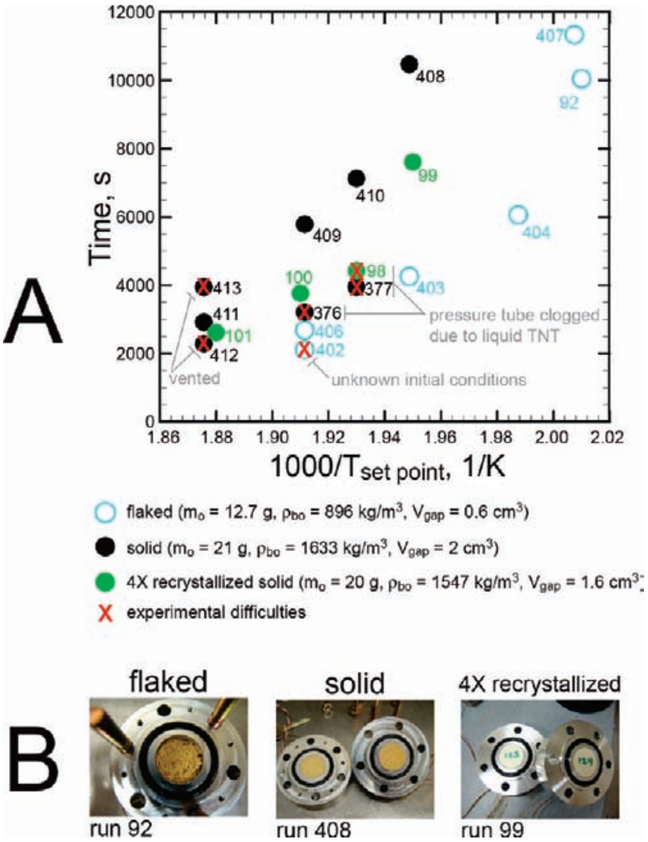

Figure 7. (A) TNT SITI data from 2006 to 2009 and (B) pictures of SITI samples.

surfaces. The level of the TNT is based on liquid TNT at 400 K, which is the temperature at 1850 s, as shown in Figure 8D.

Two stainless steel temperature probes with six thermocouples in each probe, were used to monitor the internal temperature. Data were collected with 48 thermocouples and 3 strain gauges. Figure 8C shows the average temperature measured for the base (9 thermocouples), top (9 thermocouples), and side (3 at each of 6 level for a total of 18 thermocouples) for tests 229, 231, and 233. The base, side, and top temperatures are represented by a red line, black lines, and a green line, respectively. These average temperatures were used as Dirichlet boundary conditions. Temperatures located between the thermocouples were determined with linear interpolation. The base heater supplied about 800, 300, and 100 W of power for tests 229, 231, and 233, respectively. Differences between the top and base temperatures decrease with lower heater power.

Figure 8D shows the temperatures measured with the internal probes. Temperature 6 measures the temperature in the air enclosure, which is always less than the temperature of the TNT. As the TNT melts, the temperature along the internal probe shows a temperature gradient that is hottest near the bottom of the TNT and cooler near the top of the TNT. After the TNT melts, the TNT temperature at both the center probe and outer probe locations are the same, indicating significant heat transfer caused by forced convective heat transfer associated with the decomposing TNT. After about 31 min, the TNT in test 229 is completely melted, and ignition occurs at about 63 min (3790 s).

Finite Element Mesh and Solution Method

Figure 9 shows six meshes: one ODTX mesh, three SITI meshes, and two midscale meshes. The three SITI meshes were necessary because the experiments with flaked, solid, and 4× recrystallized TNT had different expansion gap volumes. The midscale test was modeled in both two dimensions (2D) and three dimensions (3D). The mesh for the TNT in the midscale meshes represents 1.95 kg of liquid TNT at 127 °C (400 K), which is the state of the TNT after melting. Most of the midscale analyses were done with the 2D mesh. A single calculation was done with the 3D mesh.

We simplified the midscale simulation with liquid convection by starting the calculation with the TNT volume the same as the liquid TNT volume at 400 K, which is the temperature of the TNT when all of the TNT melts in accordance with Figure 8D. This assumption is equivalent to packing the flaked TNT to the same volume that would be occupied by the liquid TNT at 400 K. Modeling the change in volume of solid, liquid, and gas associated with the melting would require the solution of momentum equations for the solid, liquid, and gas, which is beyond the scope of this article.

Equations listed in Tables 1 and 3 were solved using a preconditioned conjugate gradient solver with the finite element code Calore[19] for the ODTX and SITI configurations without liquid convection. For the midscale experiment, the liquid TNT was allowed to circulate with no slip between the local gas and condensed phases. However, slip was allowed at the interface between the liquid TNT and the air enclosure. For the midscale simulation with liquid convection, the equations listed in Tables 2 and 3 were solved with the finite element code Comsol[20] using the direct solver UMFPACK.[32] The 3D model had to be solved with a coarse mesh and a segregated solver because of the large memory requirements necessary to solve the asymmetric sparse system of equations directly. The TNT material parameters for all three models were taken from Table 4. Parameters that are specific to each experiment, such as density, were taken from Table 5.

Uncertainty Analysis

Uncertainties in the calculated results for the ODTX and SITI simulations were determined using a Latin hypercube sampling (LHS) technique. The LHS technique is an efficient, constrained sampling technique developed by McKay et al.[33] and is used to propagate uncertainty into the predicted results. Ten parameters, α_c, α_g, h_{pc}, k_{fac}, T_{pc}, w_{pc}, ρ_{bo}, V_{enc}, V_{tube}, and ω_{tnt}, listed in Tables 4 and 5 vary about their nominal values. Only 8 of these 10 uncertain parameters are needed for the ODTX simulations because the enclosure volume and tube volume are zero. In the current work, only $n + 1$ samples were run for each LHS analysis. Therefore, 9 and 11 LHS runs were made for each boundary temperature for the ODTX and SITI simulations, respectively.

For the SITI analysis, the uncertainties in the 10 uncertain parameters were accounted for by selecting 11 different values for each of the 10 parameters. The range of each input parameter was divided into 11 nonoverlapping intervals on the basis of equal probability. One random value from each interval was selected according to the probability density function in the interval. The 11 values thus obtained for the first parameter were then paired in a random manner with the 11 values obtained for the second parameter. These 11 pairs were then combined in a random manner with the 11 values of third parameter to form 11 triplets and so on until 11 sets of the 10 input variables were formed. The ignition times were then calculated 11 times with the 11 different sets of input parameters.

The mean and standard deviation of the ignition times were then calculated from the 11 sets of responses. A distinct LHS

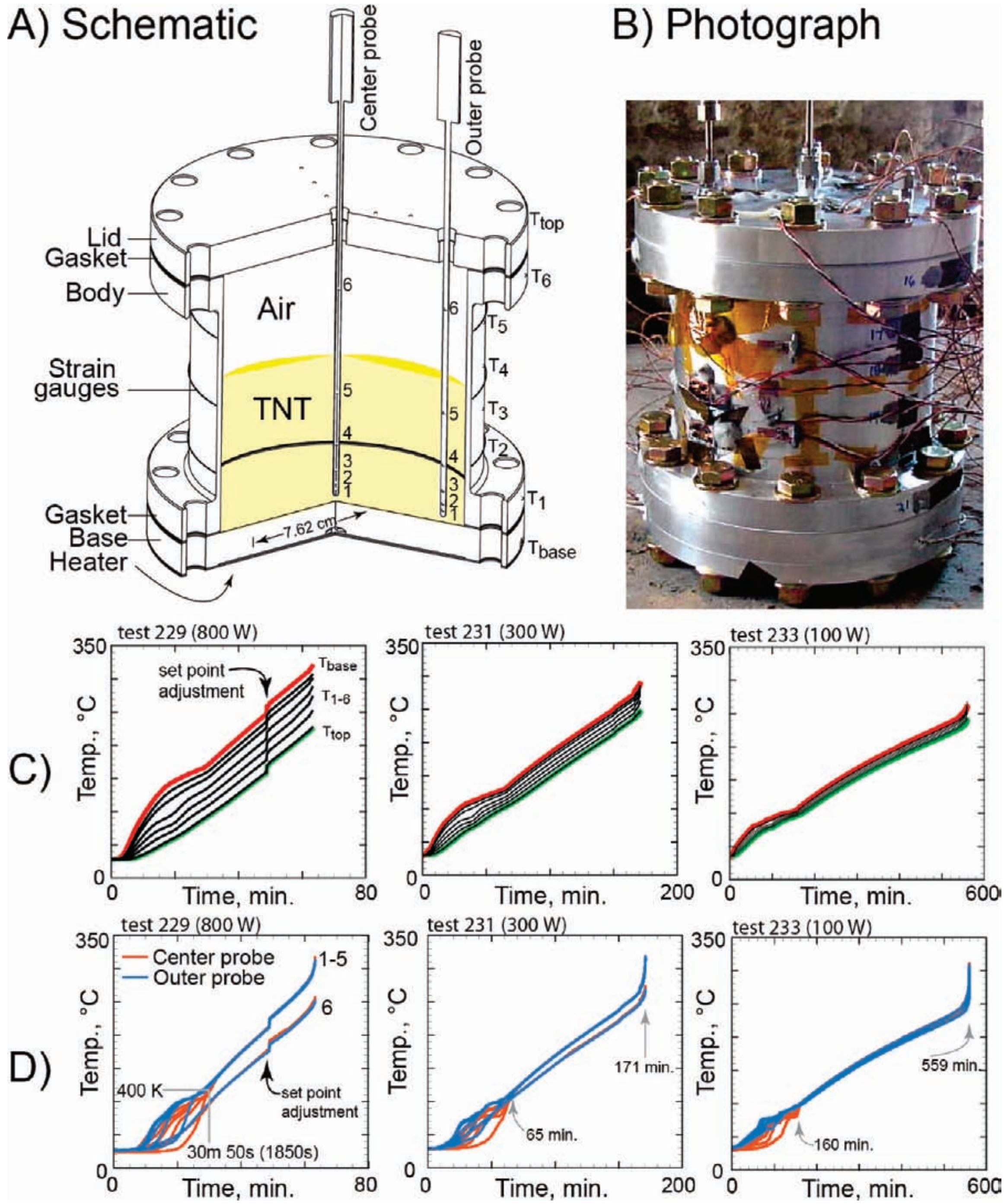

Figure 8. Midscale (A) schematic,[31] (B) photograph, (C) external, and (D) internal temperatures.

analysis was made for each new boundary temperature. Table 6 indicates that 758 simulations were run to determine the mean ignition time as a function of the applied boundary condition for the ODTX and SITI experiments using LHS. A 95% prediction limit was determined using a Student t distribution with 8 degrees of freedom for the ODTX runs ($\mu \pm 2.306\sigma$) and 10 degrees of freedom for the SITI runs ($\mu \pm 2.228\sigma$).

To measure the correlation strength or sensitivity of the ignition time, the standard linear correlation coefficient was computed for each of the uncertain input parameters, $r = ((1/(n-1))\Sigma_{i=1}^{n}(t_i - \mu_t)(y_i - \mu_y))/(\sigma_t \times \sigma_y)$, where μ_t represents the mean or average computed ignition time in the n LHS runs, μ_y is the mean of the corresponding LHS input values for the uncertain variable y, and μ_t and μ_y are the standard deviations of the response ignition time and input values. A perfect positive or negative linear correlation is $|r| = 1$. A linear correlation strength is assumed to be significant when $|r| > 0.5$ or $r^2 > 0.25$. Such judgments of r values depend on whether a linear model is a good fit of the simulation results. The examination of scatter plots of response versus parameter values is a good way to judge the strongly organized linear or nonlinear relationship between the model parameters and the model response. Mean parameter values were used for all midscale simulations.

One-Dimensional Time-to-Explosion and Sandia's Instrument Thermal Ignition Simulations

Figures 10 and 11 show comparisons between predicted and measured ignition times for all of the ODTX and SITI experiments, respectively. For each experiment, three prediction

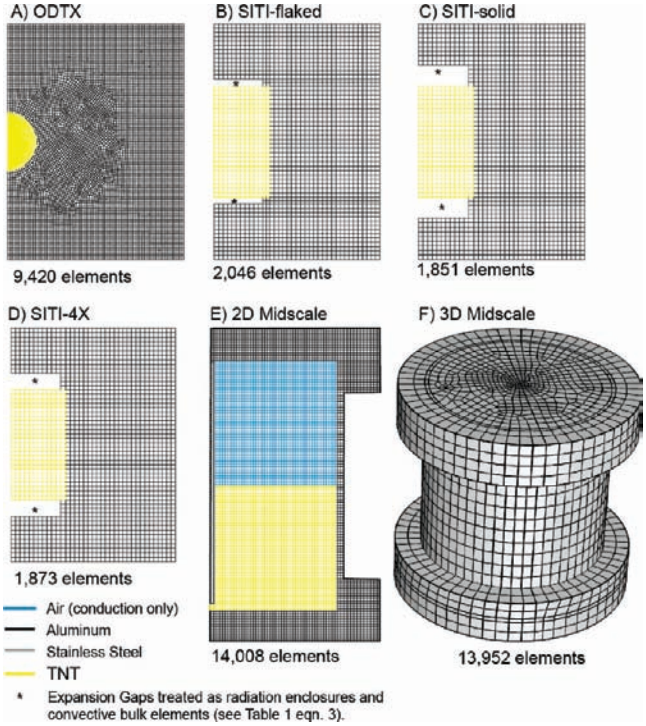

Figure 9. Two-dimensional (2D) axisymmetric meshes with quadratic elements for (A) ODTX, (B) SITI with flaked TNT, (C) SITI with solid TNT, (D) SITI with 4× recrystallized TNT, and (E) midscale after TNT has melted. (F) 3D mesh with hexagonal elements for the midscale experiment.

TABLE 6: Number of Simulations for Uncertainty Analysis

simulation[a,b]	1000/*T* range	no. LHS runs	no. simulations
ODTX (99% pure)	1.73 to 2.07	18	162
ODTX (94% pure)	1.63 to 1.91	15	135
ODTX (90% pure)	1.61 to 1.93	17	153
SITI (flaked)	1.90 to 2.01	12	132
SITI (solid)	1.88 to 1.95	8	88
SITI (4×recrystallized)	1.88 to 1.95	8	88
		total =	758

[a] 9 runs per LHS for ODTX (8 parameters with variability). [b] 11 runs per LHS for SITI (10 parameters with variability).

lines are shown. The middle line represents the mean of nine LHS samples for the ODTX experiment and the mean of eleven LHS samples for the SITI experiment. The upper and lower lines represent the 95% prediction limit, as discussed in the previous section. The measurements represent individual runs. The ODTX temperature is the temperature of the anvils. The SITI temperature is the set point temperature of the outer confinement. The temperature of the outer confinement was made to reach the set point temperature from room temperature in 15 min. The mini plots show the correlation strength of the parameters to the ignition time when 1000/*T* is 1.89. Clearly, the TNT impurity dominates the uncertainty in these predictions.

Figure 12 shows a comparison between the predicted and measured internal temperatures for various set point temperatures for the SITI experiments. The top plot shows the location of each temperature measurement on a cross section of the TNT. Figure 12 also shows the predicted and measured pressures for the SITI experiments. The top plot is for the solid SITI samples and the bottom plot is for the flaked SITI samples. The inset plots show a close-up view of the temperature as the TNT changes from a solid to a liquid. The predictions are the mean of 11 LHS samples. The measurements are single experiments and do not represent repeat runs.

Figure 13 shows the predicted gas volume fraction, effective conductivity, pressure, solid fraction, bulk density, and temperature at the center, midradius, and outer edge of a 1.27 cm diameter ODTX TNT sphere that is 99% pure. Figure 14 shows the same information for the solid TNT in SITI showing pore collapse due to phase change, followed by pore expansion due to reaction. Each color represents a different boundary temperature, as indicated in the plot legend. Most of the ODTX runs indicate center ignition. However, the temperature plots at the midradial position for the hotter anvil temperature (cyan line) indicate that ignition is not at the center. High ODTX pressures may explain the reported sizzle and smoke (indicating leakage) during many of the TNT ODTX experiments. Future ODTX experiments with TNT should use a lower initial bulk density.

Validation

The TNT ignition model was applied to the midscale experiment representing a three orders of magnitude increase in volume over the ODTX experiments. Table 7 describes several simulations that were performed with this larger volume for three different power levels supplied to the bottom of the confining vessel: 800, 300, and 100 W. Four simulations of test 229 at 800 W were used to investigate the effect of liquid convection (compare simulation 1 and 2), multiple dimensions (compare simulations 2 and 3), and increased conductivity (compare simulations 2 and 4). Two additional simulations were used to show predictive capability at reduced power levels of 300 and 100 W.

Figure 15 shows the temperature at the time of ignition for simulations 1−4 listed in Table 7. The arrows in the solutions with flow represent normalized velocities. The arrows in the solution without liquid convection represent heat flux. The magnitudes of the heat flux arrows are proportional to the maximum heat flux. Streamlines are also plotted on the 2D solution with free liquid convection.

The measured ignition time (3790 s) is close to all of the predicted ignition times for run 229. Even the solution without liquid convection gave an adequate prediction of the ignition time because the predicted flow velocity was slow, being on the order of 0.3 cm/s with a stagnation zone predicted near the bottom of the experiment. The 3D simulation in Figure 15 predicts an asymmetric ignition near the bottom of the TNT. Initially, the ignition starts on the bottom, and then the flow pushes it to one side and eventually the top. The purple isovolume shows the start of the ignition sequence. The reacted solid fraction within the purple isovolume is between 0.85 and 1.0. The predicted gas volume fraction within the purple region is between 0.3 to 15.3%. The ignition time is a few hundred seconds less than the measured ignition time. These differences are likely due the coarse mesh used in the 3D simulation.

Although the ignition times were predicted adequately for simulations 1−4, the predicted temperature in the TNT did not match the center probe measurements, as shown in Figure 16 for all six simulations. The measurements show that the temperatures at locations 1−5 are nearly the same, indicating that there is no gradient in the TNT once it has melted and reactions have commenced. In other words, the flow is not simple free liquid convection. The gradients in the TNT are less for the slower heating runs 231 and 233, and the predicted ignition times are close to the measured ignition times for these cases.

Incropera and DeWitt[24] give values of convective heat transfer coefficients that range from 2 to 100 000 W/m^{2}K for free

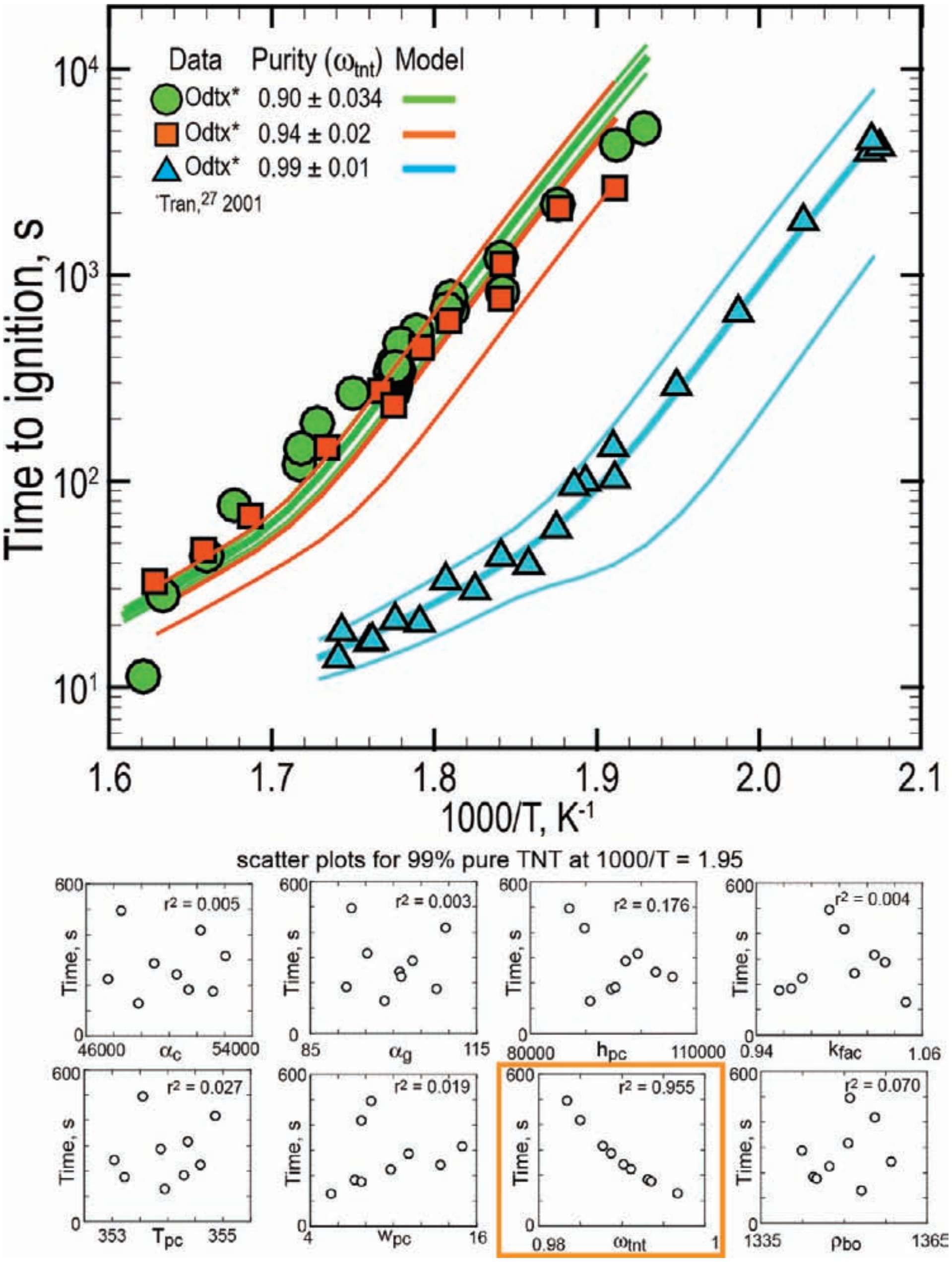

Figure 10. Predicted (lines) and measured (symbols) ignition times for the ODTX experiments. The middle lines represent the mean of nine LHS samples. The outer two lines represent the 95% prediction interval. The mini plots show scatter plots of each of the nine LHS samples for the 99% pure TNT runs when 1000/T is 1.95. Only the purity (ω_{tnt}) shows significant correlation with ignition time.

convection of gases to forced convection with phase change. Modeling three-phase (solid, liquid, and gas) reactive flow is complex and is beyond the scope of the current work. A simple method to mimic enhanced heat transfer is to increase the effective thermal conductivity substantially after the TNT melts.

The effective thermal conductivity was increased by 1000 W/mK at 1850 s after the TNT melts in simulation 4 to mimic increased heat transfer due to forced convective heat transfer. With an enhanced thermal conductivity, the TNT reaches a homogeneous temperature equal to the temperature of the hottest surface. This temperature is hotter than the measured temperature, verifying the fact that increased conduction is not sufficient to model the enhanced heat transfer caused by forced convective flow.

Although three-phase reactive heat transfer would be a desirable method to solve this complex reactive flow problem, the ad hoc method was shown to predict ignition times adequately and gives credibility to the TNT decomposition model. An alternative engineering approximation would be to add a reactive source term to the bulk element formulation (eq 7 in Table 1) and treat the TNT as a bulk element after it melts using an appropriate Nusselt number for boiling heat transfer to determine the convective heat transfer coefficient.

Summary and Conclusions

Decomposition of TNT is complicated because of its low melting point, followed by a long induction period where solid-phase reactions generate a reactive coke. The reactive coke acts as a catalyst to produce gaseous decomposition products, which lead to pressure-dependent ignition. The long induction period, followed by a rapid increase in reaction, was modeled with a single-step mechanism using a non-Arrhenius reaction rate. The reaction rate was assumed to be dependent on the square root

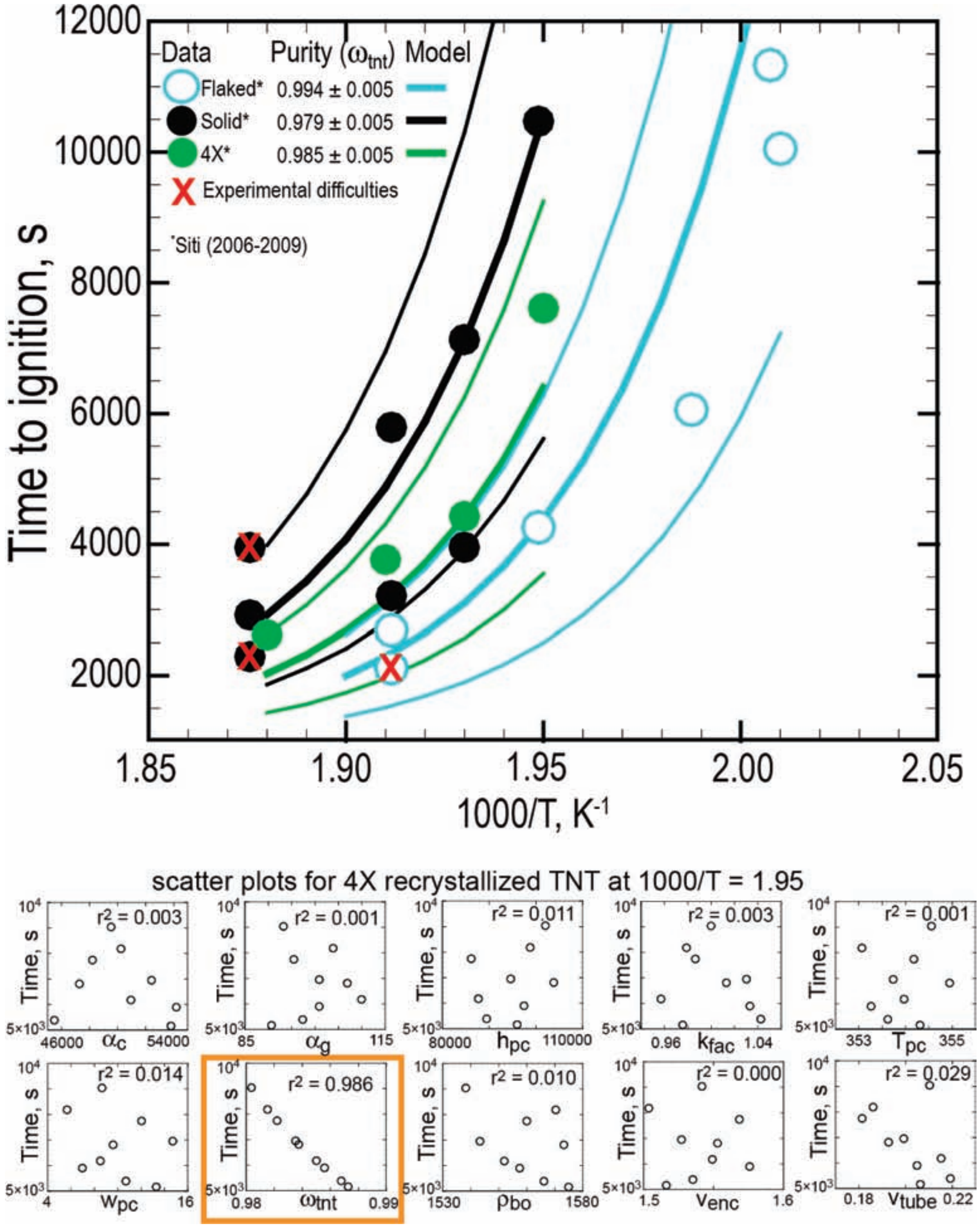

Figure 11. Predicted (lines) and measured (symbols) ignition times for the SITI experiments. The middle lines represent the mean of 11 LHS samples. The outer two lines represent the 95% prediction interval. The mini plots show scatter plots of each of the 11 LHS samples when 1000/T is 1.95. Only the purity (ω_{tnt}) shows significant correlation with ignition time.

of pressure, and the activation energy was assumed to be normally distributed with respect to the reaction progress. The decomposition products were assumed to be in chemical equilibrium. The mean activation energy was taken to be the same as the activation energy used by Brill and James[13] for the catalyst-dominated phase of the TNT decomposition.

Reaction rate coefficients were fit using data from both the ODTX and SITI experiments. Initially, the coefficients were fit with no pressure dependency. Even though the SITI data could be fit without pressure dependency, the ODTX data could not be modeled accurately with these pressure-independent rates. Because the ODTX data contained little expansion volume and the pressure increase was high, a pressure-dependent reaction mechanism fit both sets of data accurately. However, in practical systems with ample expansion volume, the pressure dependency is likely low, such as in the midscale experiments used for validation, where the pressure rise was small. Future work should determine if pressure dependency is necessary when forced convection is considered.

Previous work at shocklike pressures of 10−50 kbars indicates that TNT decomposition is pressure independent. A similar observation was made in the current work when the confining vessel contained significant free space and the pressure rise was insignificant. The current work proposes that at pressures from 1 to 2 kbars, TNT decomposition is dependent on pressure, especially for experiments without room for expansion. During the long induction period with little gas generation, rates are little affected by pressure. However, during the catalyst dominated phase of the decomposition, pressure plays a more prominent role in TNT decomposition.

Thermal conductivity at temperatures below reaction thresholds were obtained from the SITI experiments. Thermal conductivities at higher temperatures were determined using an effective thermal conductivity model that separates conductive

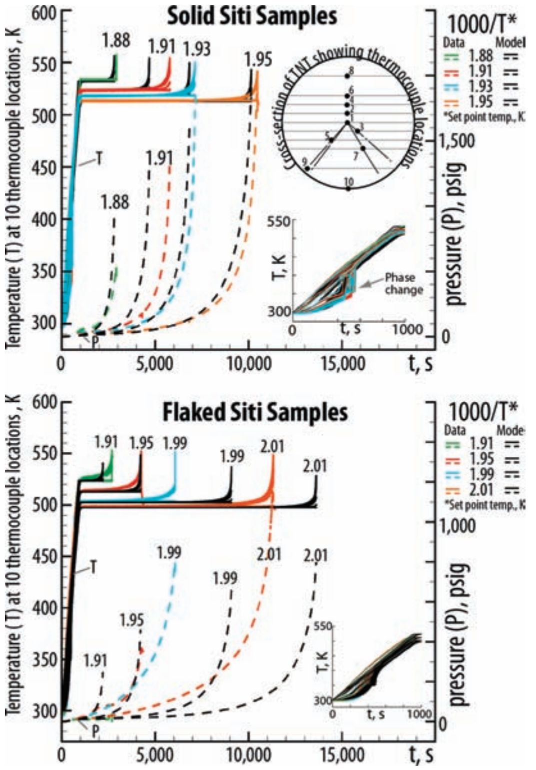

Figure 12. Predicted (black lines) and measured (colored lines) internal temperatures and pressures for the solid (top plot) and flaked (bottom plot) SITI experiments.

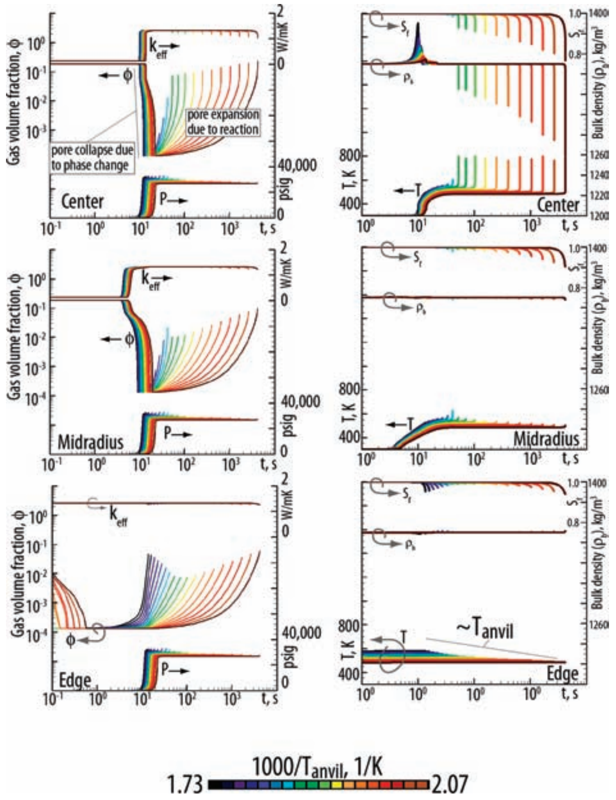

Figure 13. Predicted gas volume fraction, effective conductivity, pressure, solid fraction, bulk density, and temperature at the center, midradius, and edge of a 1.27 cm diameter TNT sphere that is 99% pure.

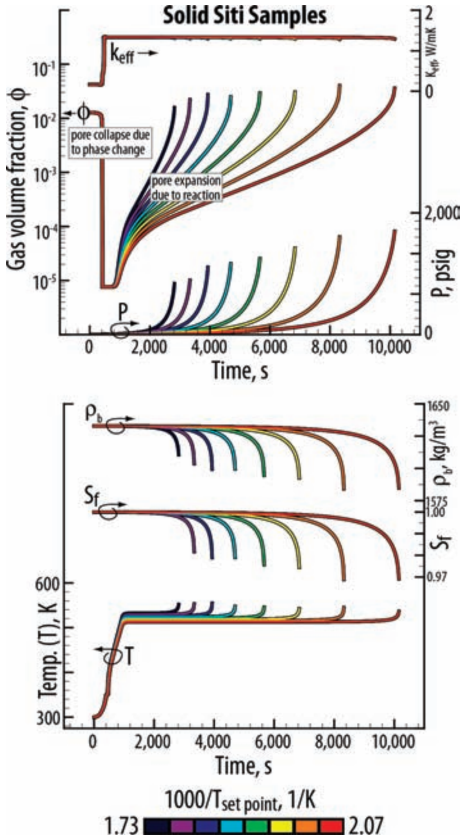

Figure 14. Predicted gas volume fraction, effective conductivity, pressure, solid fraction, bulk density, and temperature at the outer edge of a 2.54 cm diameter by 2.54 cm high cylinder of solid TNT in the SITI apparatus.

heat transfer into three parts: conduction through the condensed TNT, conduction through the gas decomposition products, and radiation through the decomposing TNT. Evolving gas volume fraction and bulk densities were calculated as field variables. We determined pressures as an integral quantity by assuming that the gas velocities were significantly less than sound speeds. Therefore, pressure was assumed to be spatially constant, but it varies in time as the TNT decomposes.

Two transport models were used to test the TNT decomposition model and the necessity of including liquid convection. Both transport models assumed that the solid and gas temperatures were the same at each spatial location. One transport model included only the overall energy and continuity equations with reaction and did not consider liquid flow. The second transport model also included the Navier−Stokes equation for the flow of the TNT. No slip was assumed between the local gaseous and condensed phases. Slip was allowed between the liquid and air interfaces. The transport model without liquid convection was applied to three scales of experiments with TNT volumes ranging from 1 to >1000 cm^3, a three-order difference in volume. The transport model with flow was applied only to the large-scale experiment. Both transport models were able to predict times-to-ignition, internal temperature measurements, and increases in pressure due to temperature and reaction.

The uncertainty of the decomposition model was determined using an LHS analysis of both the SITI and ODTX experiments. The strong effect of impurity on the time-to-ignition in the ODTX experiments, first shown by Tran et al.,[4] was modeled empirically. The rates for 99% pure TNT were decreased by a factor of 40 to match ODTX data for 90% pure TNT. The impurities in the 90% pure TNT samples were not measured and may not be typical of production grade TNT. A final validation was performed on a much larger experiment referred to as the midscale experiment.

TABLE 7: Midscale Simulations

simulation (run ID)	power, watts	measured ign. time	calculated ign. time	simulation geometry	free conv.	increased cond.[a]
1 (229)	800	1 h 2 min	1 h 4 min	2D	N	N
2 (229)	800	1 h 2 min	1 h 3 min	2D	Y	N
3 (229)	800	1 h 2 min	1 h 0 min	3D[b]	Y	N
4 (229)	800	1 h 2 min	1 h 3 min	2D	Y	Y
5 (231)	300	2 h 49 min	3 h 2 min	2D	Y	N
6 (233)	100	9 h 18 min	10 h 11 min	2D	Y	N

[a] Increased k_{eff} by 1000 W/mK after the TNT reaches 400 K to approximate forced convection effects. [b] 3D simulations show asymmetric ignition due to 3D flow effects.

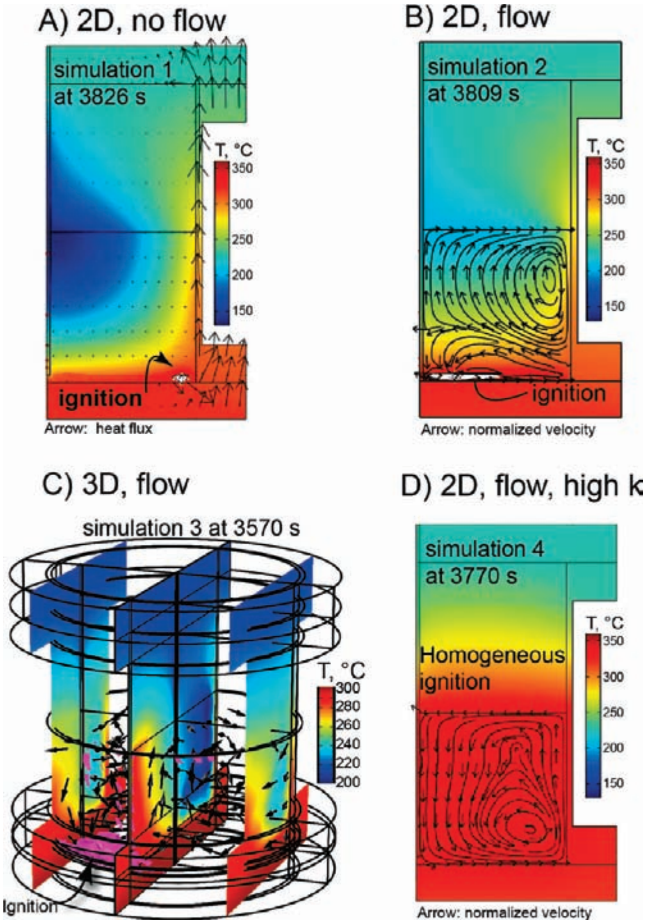

Figure 15. Simulations 1−4 of run 229 at ignition showing the effects of free liquid convection, multiple dimensions, and high thermal conductivity.

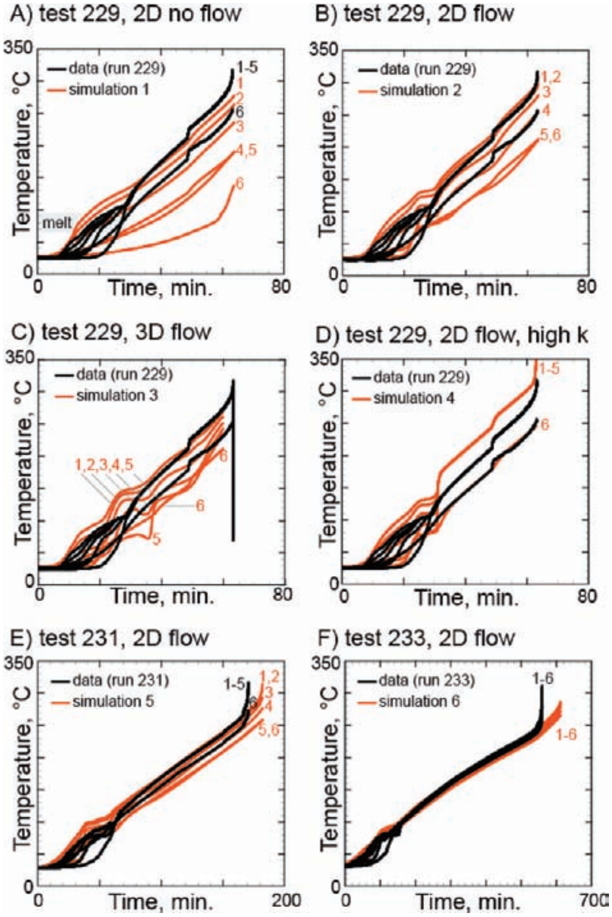

Figure 16. Measured and calculated center probe temperatures at locations 1−6 depicted in Figure 8A for the six midscale simulations.

All of the confined SITI data were within the predicted LHS confidence intervals. The SITI data included time-to-ignition for both flaked and solid TNT samples, spatially and temporally resolved temperatures, and thermodynamic pressure. The ODTX data at various levels of purity were also within the predicted LHS confidence intervals. Ignition times were also predicted quite accurately for the midscale experiment using both transport models. However, the internal temperatures were not predicted as well.

Future Work

The effect of impurity on ignition times should be investigated. The 90% pure TNT was obtained from Holston grade TNT. The impurities in this lot seem to be greater than the impurities in typical TNT formulations. The identity of the impurities should be determined and studied to see why they would slow the apparent reaction rates 40-fold. Future ODTX experiments should be performed at lower densities to avoid high pressures. Because the pressures were so high in the ODTX experiments, the ideal gas assumption was probably not valid in the current work for the ODTX experiments. Also, the temperature-dependent viscosity of TNT should be measured to temperatures higher than 100 °C, perhaps to as high as 150 °C. Better data on TNT viscosity will enable more accurate simulations of realistic geometries where flow is important. Three-phase (solid, liquid, and gas) reactive flow should be considered for future modeling efforts.

Acknowledgment. Work performed at Sandia National Laboratories (SNL). Sandia is a multiprogram laboratory operated by Sandia Corporation, a Lockheed Martin Company, for the United States Department of Energy's National Nuclear Security Administration under contract DE-AC04-94AL85000. We would like to thank Craig Tarver and Tri Tran at Lawrence Livermore National Laboratory for supplying the ODTX data for TNT, Tom Massis (SNL) for supplying the pure TNT for the SITI experiments, Stephen Chrisman (SNL) for determining the purity of the SITI samples, Dave Zerkle at Los Alamos National Laboratories (LANL) for help using Comsol, Jonathan Morgan (LANL) for the drawing of the Midscale test, Justin Dawson (SNL) for helping to organize and define the boundary conditions for the SITI and midscale tests, Michelle Steyskal (SNL) for helping to organize the midscale data, Mel Baer (SNL) for many discussions regarding energetic materials, Bill Erikson (SNL) and Will Wente (SNL) for internal review, and Imane Khalil (SNL) for management support.

References and Notes

(1) Kaneshige, M. J.; Renlund, A. M.; Schmitt, R. G.; Erikson, W. W. *Twelfth International Detonation Symposium*; ONR 333-05-2; Office of Naval Research: San Diego, CA, 2002; p 821.

(2) Catalano, E.; McGuire, R.; Lee, E.; Wrenn, E.; Ornellas, D.; Walton, J. *Sixth Symposium (International) on Detonation*; ONR ACR-221; Office of Naval Research: Coronado, CA, 1976; p 214.

(3) McGuire, R. R.; Tarver, C. M. *Seventh Symposium (International) on Detonation*; NSWC MP 82-334; Naval Surface Weapons Center, U.S. Naval Academy: Annapolis, MD, 1981; p 56.

(4) Tran, T. D.; Simpson, R. L.; Maienschein, J.; Tarver, C. *32nd International Annual Conference of Institute of Chemistry Technology*; DWS Werbeagentur & Verlag: Karlsruhe, Germany, 2001; p 25.

(5) Zinn, J.; Mader, C. L. *J. Appl. Phys.* **1960**, *31*, 323.

(6) Zinn, J.; Rogers, R. N. *J. Phys. Chem.* **1962**, *66*, 2646.

(7) Merzhanov, A. G.; Abramov, V. G. *Propellants, Explos., Pyrotech.* **1981**, *6*, 130.

(8) Dacons, J. C.; Adolph, H. G.; Kamlet, M. J. *J. Phys. Chem.* **1970**, *74*, 3035.

(9) Dobratz, B. M. *LLNL Explosives Handbook Properties of Chemical Explosives and Explosive Simulants*; Lawrence Livermore National Laboratory Report DE85-01591; 1981; p 1.

(10) Hobbs, M. L.; Baer, M. R.; McGee, B. C. *Propellants, Explos., Pyrotech.* **1999**, *24*, 269.

(11) Image of Sooty TNT Explosion. http://www.ch.ic.ac.uk/vchemlib/mim/bristol/tnt/tnt_text.htm. (accessed March 31, 2009).

(12) Lee, E. L.; Sanborn, R. H.; Stromberg, H. D. *Fifth Symposium (International) on Detonation*; Office of Naval Research Report ACR-184; Pasadena, CA, 1970; p 331.

(13) Brill, T. B.; James, K. J. *J. Phys. Chem.* **1993**, *97*, 8759.

(14) Erikson, W. W. *Thirteenth International Detonation Symposium*; ONR 351-07-01; Office of Naval Research: Norfolk, VA, 2006; p 629.

(15) Pitt, G. J. *Fuel* **1962**, *41*, 267.

(16) Hobbs, M. L. *Polym. Degrad. Stab.* **2005**, *89*, 353.

(17) Hobbs, M. L.; Kaneshige, M. J. *Thirteenth International Detonation Symposium*; ONR 351-07-01; Office of Naval Research: Norfolk, VA, 2006; p 507.

(18) Hobbs, M. L.; Steyskal, M.; Kaneshige, M. J. In *JANNAF 24th Propulsion Systems Hazards Meeting*; Boston, MA, 2008; p 1.

(19) Bova, S. W.; Copps, K. D.; Newman, C. K. *Calore: A Computational Heat Transfer Program*; Sandia National Laboratories Report SAND2006-6083P; 2006; p 1.

(20) COMSOL: Multiphysics Modeling. http://www.comsol.com/. (accessed November 25, 2008).

(21) Glicksman, L. R. Heat Transfer in Foams (Chapter 5). In *Low Density Cellular Plastics*; Hilyard, N. C., Cunningham, A., Eds.; Chapman and Hall: London, U.K., 1994; p 104.

(22) Gibson, L. J.; Ashby, M. F. *Cellular Solids Structure and Properties*, 2nd ed.; Cambridge University Press: Cambridge, U.K., 1997; p 289.

(23) Siegel R.; Howell, J. R. *Thermal Radiation Heat Transfer*, 3rd ed.; Taylor & Francis: Washington, DC, 1992; p. 527.

(24) Incropera F. P.; DeWitt, D. P. *Fundamentals of Heat and Mass Transfer*, 5th ed.; John Wiley & Sons: New York, 2002; p 1.

(25) *LASL Explosive Property Data*; Gibbs, T. R., Popolato, A., Eds.; University of California Press: Los Angeles, CA, 1980; p 172.

(26) *Military Explosives*; Department of the Army Technical Manual TM 9-1300-214; Headquarters, Department of the Army: Washington, DC, 1984; p 1.

(27) Tran, T. D., Lawrence Livermore National Laboratory, private communication, 2008.

(28) Zerkle, D. K. *Thirteenth International Detonation Symposium*; ONR 351-07-01; Office of Naval Research: Norfolk, VA, 2006; p 771.

(29) Chrisman, S. C. Sandia National Laboratories, private communication, 2008.

(30) Marley. *SEM Annual Conference & Exposition on Experimental and Applied Mechanics*, Albuquerque, NM, 2009; p 1.

(31) Morgan, J. Los Alamos National Laboratories, personal communication, 2004.

(32) Davis, T. A. *ACM Transaction on Mathematical Software* **2004**, *30*, 196.

(33) McKay, M. D.; Conover, W. J.; Beckman, R. J. *Technometrics* **1979**, *21*, 239.

JP906134F